2024 IEEE International Conference on Robotics and Automation (ICRA 2024)
May 13-17, 2024. Yokohama, Japan

Towards a Novel Soft Magnetic Laparoscope for Single Incision Laparoscopic Surgery

Hui Liu[1], Ning Li[1], Shuai Li[1], Gregory J. Mancini[2] and Jindong Tan[1]

***Abstract*— In single-incision laparoscopic surgery (SILS), magnetic anchoring and guidance system (MAGS) is a promising technique to prevent clutter in the surgical workspace and provide a larger vision field. Existing camera designs mainly rely on rigid structure design, resulting in risks of losing magnetic coupling and impacting tissue during the insertion and coupling procedure. In this paper, we proposed a wireless MAGS consisting of soft material and structure design. The camera can bend at the exit of the trocar and maintain strong coupling with the external actuator. The operation principle and modeling were established to investigate the parameter design. An easier insertion procedure was introduced and demonstrated in the experiment. The bendability was tested showing the camera could reach 20° in bending angle and $16.4mm$ in displacement. The insertion and deployment took less than 2 minutes on average.**

I. INTRODUCTION

In single-incision laparoscopic surgery (SILS), surgeons can execute intricate procedures within the human body cavity through a solitary keyhole incision. This method presents advantages such as minimal scarring and expedited recovery [1]. Nevertheless, SILS encounters trocar crowding, which complicates the procedure and limits the field of view (FOV) of laparoscopes.

To address the above issues, Cadeddu [2] proposed the concept of a magnetic anchoring and guidance system (MAGS), in which a camera embedded with magnets is inserted into the patient's abdomen and anchored against the abdominal wall with a magnetic actuator outside the body. By substituting rigid linkages with magnetic coupling, the internal camera can be maneuvered to a desired position, thereby releasing the port for additional instruments. Drawing inspiration from MAGS, numerous conceptual designs concerning magnetically driven laparoscopes have been formulated and assessed in trans-abdominal operations [3], [4], [5], [6], [7], [8], [9]. Recent research efforts have concentrated on the development of intra-abdominal laparoscopes propelled solely by magnetic interaction [10], [11], [12]. Our group has conceptualized and built an untethered robotic laparoscope system featuring a camera endowed with four degrees of freedom (DOFs), alongside functionalities for wireless video transmission and control communication [13], [14], [15].

[1]Hui Liu (corresponding author), Ning Li, Shuai Li and Jindong Tan are with the Department of Mechanical, Aerospace and Biomedical Engineering, University of Tennessee, Knoxville, TN 37996, USA hliu58@vols.utk.edu, ning@vols.utk.edu, sli48@utk.edu, tan@utk.edu

[2]Gregory J. Mancini is with Graduate School of Medicine, University of Tennessee, Knoxville, TN 37920, USA gmancini@mc.utmck.edu

Currently, most designs follow a rigid stick form. One major challenge of the existing camera systems is how to define an effective and convenient insertion and deployment procedure. In [16] and [10], a standard laparoscope was inserted through an extra trocar to assist in guiding the mounting of the proposed camera devices. As for the tethered devices in [5] and [7], purse-string sutures had to be completed to seal the tissue around the wires and avoid gas escape from the insufflated abdomen. The insertion procedure became time-consuming and tedious. Tognarelli introduced an endoluminal robotic platform consisting of a shape memory alloy actuated magnetic frame for MIS. The deployment and retraction procedure took an average of 30 minutes during the tests [4].

Soft robotics have emerged as a promising technique that offers the ability to expand, twist, and bend, making them ideal candidates for next-generation instruments for SILS [17], [18], [19], [20]. Meanwhile, magnetic actuation presents an ideal solution for soft wireless devices, given that the actuating fields can effortlessly and safely penetrate most biological materials without necessitating tethers. [21]. They were successfully used in endoscope designs for drug delivery, gastrointestinal tract, and MIS applications [22], [23], [24].

In this paper, we propose a soft intra-abdominal wireless laparoscope with a safe and easy insertion process. The soft silicone rubber material was combined with our previous camera designs [13], [14], [15], enabling the camera to bend at the exit of the trocar and maintain strong coupling with the external actuator during the whole insertion process. The relationship between bending capacity and the magnetic coupling force is established to assess the component layout and selection. The bendability and the deployment procedure were evaluated by experiments. The rest of the paper is organized as follows: section II formulates the insertion problem with an overview of the camera system; section III describes the modeling and analysis for bendability; section IV shows the fabrication, demonstration, and evaluation; conclusions and future work are presented in section V.

II. PROBLEM STATEMENT

A. Overview of the Laparoscopic System

The wireless laparoscope is tailored for integration within a robotic-assisted surgical (RAS) system, as depicted in Fig. 1. This RAS system encompasses a fully insertable wireless camera, an external actuator, a force-torque sensor, and a multi-DOF manipulator. The camera and actuator are integrated with two permanent magnet pairs, which generate

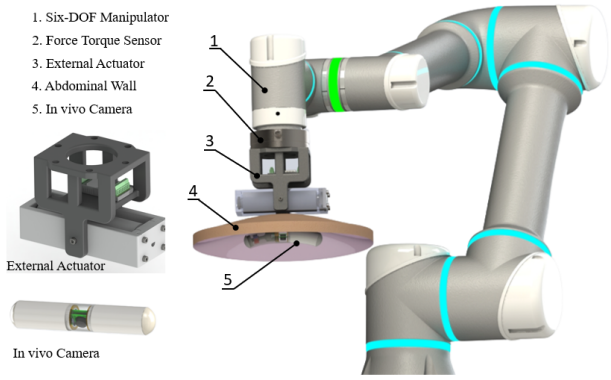

Fig. 1: The proposed wireless laparoscopic camera works as a subsystem of the robotic surgical assistant system, including an external actuator and in vivo camera module.

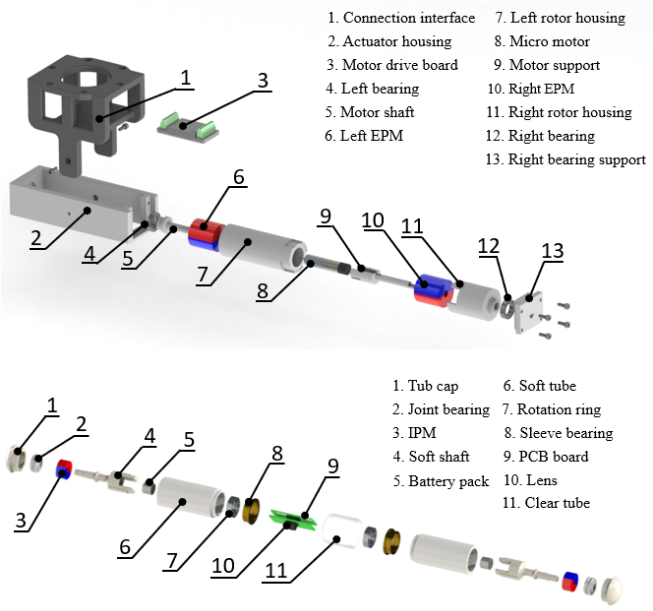

Fig. 2: Assembly exploded view of the actuator and the camera.

a magnetic coupling force that allows the camera to be anchored and navigated against the abdominal wall after being inserted through a trocar. The surgeon can manually drag the collaborative manipulator to control the external actuator during the surgery and reposition the camera to a desired pose, leaving the port free for other surgical instruments. The force-torque sensor monitors the magnetic force to ensure sufficient coupling and avoid excessive pressure on tissue.

Figure 2 illustrates the assemblies of both the actuator and the wireless camera. The camera's design comprises two internal permanent magnets (IPMs), ball bearings, soft shafts, silicone rubber tubes, battery packages, sleeve bearings, a PCB board, a lens, and a clear PVC tube. Notably, the camera's internal structure exhibits symmetry. The IPMs are positioned at each end to engage with external permanent magnets (EPMs) embedded in the external actuator. The camera board, housing sensors and chips, is secured by two sleeve bearings. Furthermore, two soft shafts, crafted from silicone rubber and accommodating the IPMs and battery packages, are upheld by ball bearings and sleeve bearings. Collaborating with soft tubes, they confer bendability to the camera, easing its insertion process.

On the other hand, the external actuator comprises a connection interface component for attaching the housing to the force-torque sensor and subsequently linking it to the manipulator. Within the actuator, two EPMs are inserted into the rotor housing, which is bolstered by two ball bearings and capable of rotating inside the actuator housing. A micromotor is seamlessly integrated into the rotor to regulate the rotation of the EPMs relative to the housing. The motor is governed by a driver board affixed to the connection interface part.

B. Insertion procedure

The insertion procedure poses a challenge for most existing rigid camera designs. General problems encountered during insertion are depicted in Fig.3a and Fig.3b. As the camera is inserted through a trocar, the magnetic coupling weakens due to the increasing distance between the EPM and IPM. Maintaining a strong EPM to sustain the coupling is essential but presents safety concerns. Even if the magnetic coupling holds until the camera is fully inserted, the front end of the camera tends to impact tissue while the rear end risks falling. To circumvent this issue, special instruments with an additional laparoscope, are typically employed to assist insertion.

In contrast, the proposed insertion procedure facilitated by soft structure design is depicted in Fig.3c and Fig.3d. As the camera emerges from the trocar, magnetic coupling between one pair of EPM and IPM is established at the front end. Throughout the insertion process, the camera bends due to magnetic attraction, maintaining a nearly constant coupling distance and stable magnetic coupling. As the camera nears full insertion, the actuator rotates around the coupling end, establishing coupling at the other end. This entire process is safe, rapid, and obviates the need for additional custom instruments.

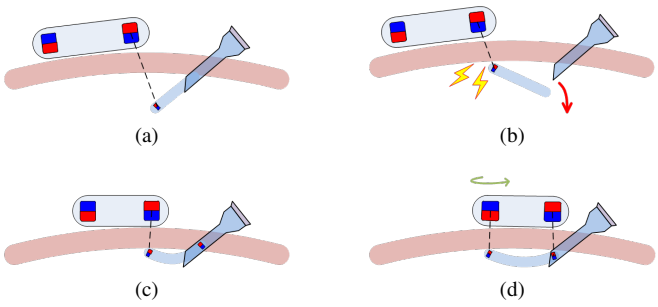

Fig. 3: **a** The magnetic coupling becomes weaker as the coupling distance increases. **b** The front end tends to impact the tissue while the tail end turns to fall. **c** The coupling distance is almost constant, and the magnetic coupling remains stably. **d** Establish of double-side.

III. MODELING APPROACH

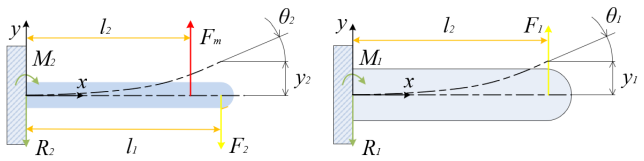

(a) Soft shaft. (b) Soft tube.

Fig. 4: Loading diagram of the soft shaft and the soft tube.

In this section, the bendability of the camera is modeled based on the cantilever beam model. Assisted with the proposed model, we notice the bendability of the camera is affected by the magnetic moment of the IPM, the material of the soft tube and soft shaft, and the position of the IPMs and ball bearings. The relationship between the magnetic coupling force and the bending angle and vertical displacement is formulated.

As shown in Fig. 4, assuming the tube and shaft can not rotate around the x axis, they can be modeled with a cantilever beam, where one end of the beam is fixed while the other end is free. M_1 and M_2 represent the reaction moment from the sleeve bearings applied to the soft tube and the soft shaft respectively. R_1 and R_2 are the reaction forces also generated by the sleeve bearing. F_m is the magnetic force applied to the IPM. F_1 and F_2 are the reaction forces between the soft tube and the soft shaft on the free end passed by the ball bearings. θ and y represent the bending angle and displacement of the free end relative to the fixed end. The reaction forces and moments R_1, R_2, M_1 and M_2 are solved by

$$\begin{cases} \sum F_y = 0 \\ \sum M_O = 0 \end{cases} \tag{1}$$

where l_1 and l_2 represent the positions of the free end and the IPM relative to the fixed end of the tube.

In this section, singularity functions were used to represent the loads on the beam model and are denoted by a binomial in angled brackets. x is the distance along the beam length. a denotes where in x the singularity function either acts or begins to act. Accordingly, the bending angle and displacement of any point on the soft shaft and soft tube relating to x are obtained in equation 2 and equation 3, where E_2 and E_1 are the Young's modulus relating to the material. I_2 and I_1 are the inertia moments concerning to the shape and bending direction.

Since the free ends of the tube and the shaft are connected by the ball bearings, we can assume the reaction forces and the displacements at the free end are equal. The reaction forces F_1 and F_2 at free end are solved as

$$F_1 = F_2 = \frac{E_1 I_1 F_m \left(3 l_1 l_2^2 - l_2^3\right)}{2 l_1^3 \left(E_1 I_1 + E_2 I_2\right)} \tag{4}$$

Substituting F_1 into $y_1(l_1)$ and $\theta_1(l_1)$, the bending angle and displacement of the camera free end are solved as

$$\begin{aligned} y_1\left(l_1\right) &= \frac{F_m \left(3 l_1 l_2^2 - l_2^3\right)}{6 \left(E_1 I_1 + E_2 I_2\right)} \\ \theta_1\left(l_1\right) &= \frac{F_m \left(3 l_1 l_2^2 - l_2^3\right)}{4 l_1 \left(E_1 I_1 + E_2 I_2\right)} \end{aligned} \tag{5}$$

IV. EXPERIMENTS AND RESULTS

A. Fabrication of the prototype

The prototyped camera ($length \times diameter = 100mm \times 20mm$) is demonstrated in Fig. 5. The ball bearings, IPMs, and clear tubes are all off-shelf products. The soft shafts and tubes are fabricated through silicone rubber mold casting, a method known for its cost-effectiveness and simplicity. To support the weight of the heaviest components, such as the IPMs and batteries, which possess relatively smaller cross-sectional areas and moments of inertia, the shafts employ a stiffer material (Smooth-Sil™ 945, SMOOTH-ON). Meanwhile, the soft tubes are crafted from biocompatible silicone rubber (Dragon Skin™ 20, SMOOTH-ON). These soft tubes, along with clear PVC tubes and caps, collectively create an enclosure space, sealing all components within the camera. With the exception of the camera board, all components are inexpensive and can be treated as surgical consumables, streamlining the preparation and sterilization process.

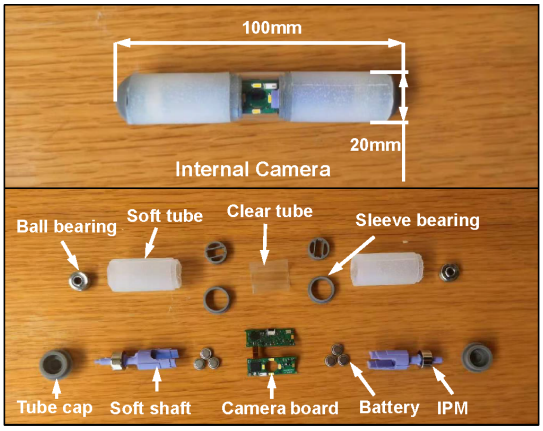

Fig. 5: The prototyped camera is compact and can be easily assembled.

B. Experimental setup

Two ex vivo experiments were conducted to evaluate the bendability and insertion procedure. The scenarios are illustrated in Fig. 6. First, the bendability of the camera was assessed by measuring the relationship between the bending angle and the applied magnetic coupling force. Second, the insertion procedure for the soft design was demonstrated to validate the feasibility.

The bendability of the camera structure offers insights into its characteristics and aids in defining the operation and insertion procedure. The experimental setup involved a fixation frame for mounting the camera module, with an aluminum profile structure supporting a benchmark displaying angles

$$\theta_2(x) = \frac{1}{E_2 I_2}\left[M_2 < x-0 >^1 - \frac{R_2}{2} < x-0 >^2 + \frac{F_m}{2} < x-l_2 >^2 - \frac{F_2}{2} < x-l_1 >^2\right]$$
$$y_2(x) = \frac{1}{E_2 I_2}\left[\frac{M_2}{2} < x-0 >^2 - \frac{R_2}{6} < x-0 >^3 + \frac{F_m}{6} < x-l_2 >^3 - \frac{F_2}{6} < x-l_1 >^3\right] \quad (2)$$

$$\theta_1(x) = \int \frac{M(x)}{E_1 I_1} dx = \frac{1}{E_1 I_1}\left[M_1 < x-0 >^1 - \frac{R_1}{2} < x-0 >^2 + \frac{F_1}{2} < x-l_1 >^2\right]$$
$$y_1(x) = \int \theta(x) dx = \frac{1}{E_1 I_1}\left[\frac{M_2}{2} < x-0 >^2 - \frac{R_1}{6} < x-0 >^3 + \frac{F_1}{6} < x-l_1 >^3\right] \quad (3)$$

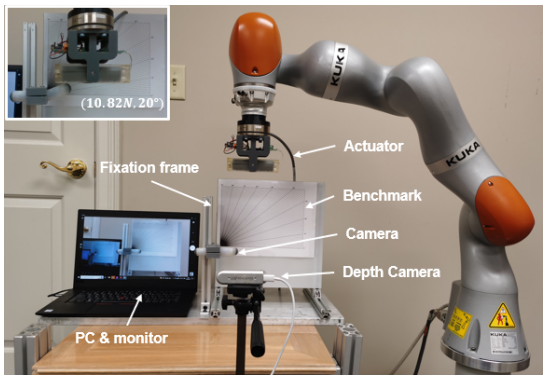

(a) Validation of bendability of the camera design.

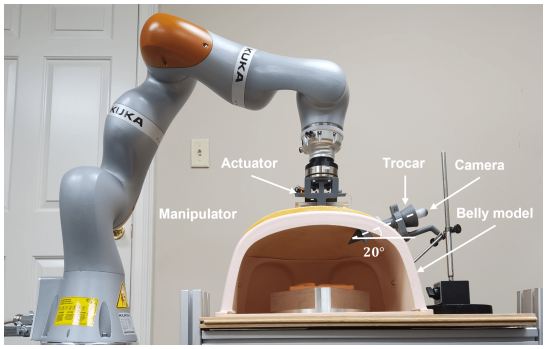

(b) Demonstration of the insertion.

Fig. 6: Experimental setup.

ranging from 0° to 90°. The origin was aligned with the bending center of the camera. During the experiment, a 7-DOF collaborative manipulator (LBR iiwa 7 R800, KUKA) controlled the actuator to approach the camera module vertically, utilizing one EPM embedded in the actuator to attract the IPM inside the camera. Simultaneously, a force-torque sensor continuously measured the coupling force, while a depth camera (RealSense™ D435, Intel) positioned in front of the scenario recorded the bending angle. The maximum bending angle and the relationship between the bending angle and coupling force were documented.

The insertion procedure commenced with inserting the camera module into the trocar mounted on a 3-Dmed synthetic human belly model. The trocar could be secured at any angle lower than the maximum bending angle of the camera. Subsequently, following a predefined procedure, the actuator was maneuvered by the manipulator to approach the camera and establish coupling between the magnets. Finally, the camera was positioned appropriately, freeing the trocar for the insertion of other instruments. Ten trials were conducted, and the time taken for each step was recorded to assess performance.

C. Bendability of soft structure

The bendability test results are shown in Fig. 7. As the coupling force increased from $0N$ to $10.82N$, the camera's bending angle reached the maximum angle of 20°. The Maximum displacement of the tube cap along the vertical direction was $16.4mm$. Ten points mapping the relation between coupling force and bending angle were recorded and represented as blue circles. The red line is the estimation based on the linear model and component properties discussed in section III. The green line is the fitted results based on the measured points. The average error is less than 3°. The error between the two lines increases when the EMP and IPM get closer and the coupling force becomes larger. Overall, the two lines stay close to each other proving the proposed model can be used to roughly estimate the bendability of the camera in the design phase.

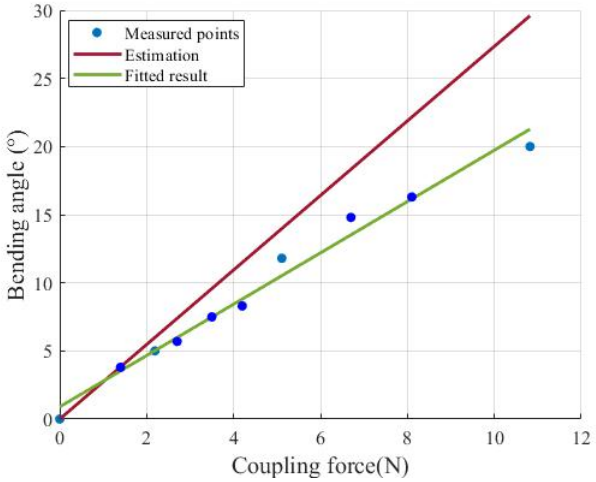

Fig. 7: Bendability test results.

D. Demonstration of insertion procedure

The insertion procedure was demonstrated ten times, resulting in an average total operation time of 118 seconds. The process of one trial and the duration of the four main steps were recorded and presented in Fig. 8 and Fig. 9. During the first step, the camera slid slowly into the trocar and approached the external permanent magnet (EPM) of the actuator. The second step, averaging 45 seconds, involved controlling the actuator to attract and gently pull the camera until its other end reached the trocar exit. Manipulator operation was constrained to a relatively low speed, with the force-torque sensor continuously monitoring the coupling force to prevent connection breakage. Subsequently, in the third step, averaging 33 seconds, the actuator was rotated around the coupling end until magnetic coupling was established on both ends. In the final deployment step, the camera was fully extracted from the trocar and maneuvered to the center of the belly model to provide an appropriate field of view (FOV), requiring an average of 22 seconds. Except for the second step, which demanded relatively delicate operation, the other steps exhibited similar durations with minor variations across each trial.

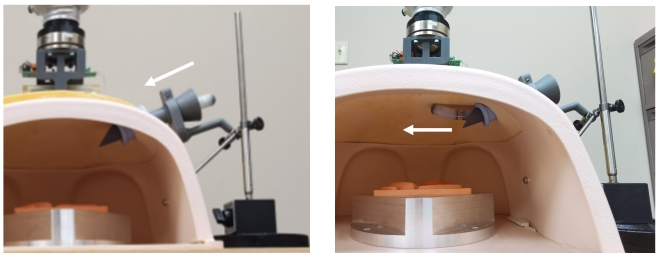

(a) Start insertion (b) Single-side coupling

(c) Double-side coupling (d) Finish deployment

Fig. 8: The four main steps of the insertion procedure were recorded.

V. CONCLUSION AND FUTURE WORK

In the present study, we introduced a soft intra-abdominal wireless laparoscope with a safe and fast insertion process. The camera can bend at the exit of the trocar to maintain the distance and coupling force during the insertion. A double-side coupling is established to avoid impacting and dropping. The whole process took less than 2 minutes on average without the assistance of an additional instrument and laparoscope. Besides, all the components, except for the camera board, are inexpensive and can be treated as

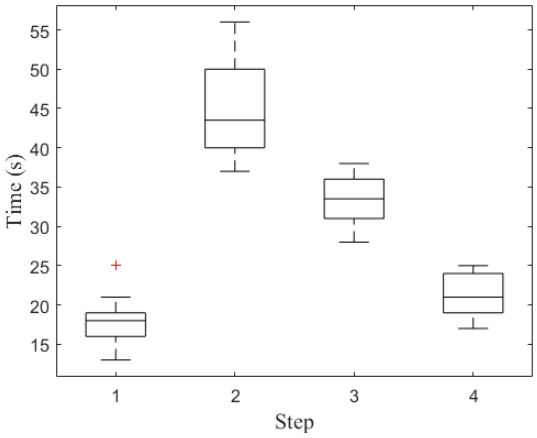

Fig. 9: Boxplots presenting the time of each step of the insertion procedure.

disposable surgical consumables. These features save the preoperative preparation time of the laparoscope system and are vital for the practical application of the system from prototype to product. As a part of future work, we plan to (a) design a new external actuator with an enclosed frame that can be sterilized, (b) explore the technical solution for 3D environmental reconstruction of the cavity, (c) optimize the selection and layout of the components inside the camera and actuator to improve the bendability of the camera, and (d) investigae strategy to clean the lens when it's contaminated by blood or other tissue.

REFERENCES

[1] L. Y. Wu and D. C. C. Foo, "Single-incision laparoscopic surgery: an update of current evidence," *Annals of Laparoscopic and Endoscopic Surgery*, vol. 1, no. 7, 2016.

[2] J. Cadeddu, R. Fernandez, M. Desai, R. Bergs, C. Tracy, S.-J. Tang, P. Rao, M. Desai, and D. Scott, "Novel magnetically guided intra-abdominal camera to facilitate laparoendoscopic single-site surgery: initial human experience," *Surgical endoscopy*, vol. 23, pp. 1894–1899, 2009.

[3] S. R. Platt, J. A. Hawks, and M. E. Rentschler, "Vision and task assistance using modular wireless in vivo surgical robots," *IEEE Transactions on Biomedical Engineering*, vol. 56, no. 6, pp. 1700–1710, 2009.

[4] S. Tognarelli, M. Salerno, G. Tortora, C. Quaglia, P. Dario, and A. Menciassi, "An endoluminal robotic platform for minimally invasive surgery," in *2012 4th IEEE RAS & EMBS International Conference on Biomedical Robotics and Biomechatronics (BioRob)*, pp. 7–12, IEEE, 2012.

[5] B. S. Terry, Z. C. Mills, J. A. Schoen, and M. E. Rentschler, "Single-port-access surgery with a novel magnet camera system," *IEEE transactions on biomedical engineering*, vol. 59, no. 4, pp. 1187–1193, 2012.

[6] M. Simi, M. Silvestri, C. Cavallotti, M. Vatteroni, P. Valdastri, A. Menciassi, and P. Dario, "Magnetically activated stereoscopic vision system for laparoendoscopic single-site surgery," *IEEE/ASME Transactions on Mechatronics*, vol. 18, no. 3, pp. 1140–1151, 2012.

[7] I. Rivas-Blanco, C. López-Casado, C. J. Pérez-del Pulgar, F. Garcia-Vacas, J. Fraile, and V. F. Muñoz, "Smart cable-driven camera robotic assistant," *IEEE Transactions on Human-Machine Systems*, vol. 48, no. 2, pp. 183–196, 2017.

[8] X. Liu, H. Liu, and J. Tan, "Towards a generic in vivo in situ camera lens cleaning module for laparoscopic surgery," in *2019 IEEE/RSJ International Conference on Intelligent Robots and Systems (IROS)*, pp. 6290–6295, IEEE, 2019.

[9] X. Liu, H. Liu, and J. Tan, "Mesoscale shape memory alloy actuator for visual clarity of surgical cameras in minimally invasive robotic surgery," *IEEE Transactions on Medical Robotics and Bionics*, vol. 1, no. 3, pp. 135–144, 2019.
[10] N. Garbin, P. R. Slawinski, G. Aiello, C. Karraz, and P. Valdastri, "Laparoscopic camera based on an orthogonal magnet arrangement," *IEEE Robotics and Automation Letters*, vol. 1, no. 2, pp. 924–929, 2016.
[11] T. Cheng, W. Li, C. S. H. Ng, P. W. Y. Chiu, and Z. Li, "Visual servo control of a novel magnetic actuated endoscope for uniportal video-assisted thoracic surgery," *IEEE Robotics and Automation Letters*, vol. 4, no. 3, pp. 3098–3105, 2019.
[12] W. Li, T. Cheng, M. Ye, C. S. H. Ng, P. W. Y. Chiu, and Z. Li, "Kinematic modeling and visual servo control of a soft-bodied magnetic anchored and guided endoscope," *IEEE/ASME Transactions on Mechatronics*, vol. 25, no. 3, pp. 1531–1542, 2020.
[13] N. Li, G. J. Mancini, and J. Tan, "Hardware design for a cable-free fully insertable wireless laparoscopic robotic camera," in *2016 38th Annual International Conference of the IEEE Engineering in Medicine and Biology Society (EMBC)*, pp. 5128–5131, IEEE, 2016.
[14] N. Li, H. Liu, R. Y. Abdolmalaki, G. J. Mancini, and J. Tan, "s-cam: an untethered insertable laparoscopic surgical camera robot with non-contact actuation," *Sensors*, vol. 22, no. 9, p. 3405, 2022.
[15] H. Liu, N. Li, G. J. Mancini, and J. Tan, "Magnetic localization for an intra-abdominal wireless laparoscope," in *2022 IEEE International Conference on Robotics and Biomimetics (ROBIO)*, pp. 135–140, IEEE, 2022.
[16] T. Hu, P. K. Allen, N. J. Hogle, and D. L. Fowler, "Insertable surgical imaging device with pan, tilt, zoom, and lighting," *The International Journal of Robotics Research*, vol. 28, no. 10, pp. 1373–1386, 2009.
[17] Y. Elsayed, A. Vincensi, C. Lekakou, T. Geng, C. Saaj, T. Ranzani, M. Cianchetti, and A. Menciassi, "Finite element analysis and design optimization of a pneumatically actuating silicone module for robotic surgery applications," *Soft Robotics*, vol. 1, no. 4, pp. 255–262, 2014.
[18] F. Connolly, P. Polygerinos, C. J. Walsh, and K. Bertoldi, "Mechanical programming of soft actuators by varying fiber angle," *Soft Robotics*, vol. 2, no. 1, pp. 26–32, 2015.
[19] B. Gorissen, M. De Volder, and D. Reynaerts, "Chip-on-tip endoscope incorporating a soft robotic pneumatic bending microactuator," *Biomedical microdevices*, vol. 20, pp. 1–7, 2018.
[20] M. Runciman, A. Darzi, and G. P. Mylonas, "Soft robotics in minimally invasive surgery," *Soft robotics*, vol. 6, no. 4, pp. 423–443, 2019.
[21] W. Hu, G. Z. Lum, M. Mastrangeli, and M. Sitti, "Small-scale soft-bodied robot with multimodal locomotion," *Nature*, vol. 554, no. 7690, pp. 81–85, 2018.
[22] D. Son, H. Gilbert, and M. Sitti, "Magnetically actuated soft capsule endoscope for fine-needle biopsy," *Soft robotics*, vol. 7, no. 1, pp. 10–21, 2020.
[23] L. N. Pham, J. A. Steiner, K. K. Leang, and J. J. Abbott, "Soft endoluminal robots propelled by rotating magnetic dipole fields," *IEEE Transactions on Medical Robotics and Bionics*, vol. 2, no. 4, pp. 598–607, 2020.
[24] T. Cheng, X. Zhang, C. S. H. Ng, P. W. Y. Chiu, and Z. Li, "Design and evaluation of a soft-bodied magnetic anchored and guided endoscope," *Journal of Medical Robotics Research*, vol. 3, no. 03n04, p. 1841007, 2018.